functions (p_y on O, p_x on O, p' on C, lobe conventions as before)

$$|n\rangle \simeq p_y; \qquad |\pi^*\rangle \simeq c_x p_x - c' p' \ (c_x, c' > 0) \tag{38}$$

Writing

$$Q^\circ = \langle p_x | Q_{xy} | p_y \rangle \tag{39}$$

it follows that

$$R_z(dc) = -K_c(\hbar e^2 c_x^2 Q^\circ / 2m_e)[XYZ]r^{-4} \tag{40}$$

This represents the CD spectrum–structure relationship for the CD of the n → π transition of a carbonyl group of assumed C_{2v} symmetry.* It yields the correct octant behavior, both in functional form and absolute sign of the octants. It also demonstrates that the background carbonyl n → π* CD may be expected to be markedly weaker than that of the pyridyl n transition; this follows from noting that the s and p overlap regions lead to higher densities than the p_x, p_y overlap, and thus the pyridine μ° moment will have a more significant effect than the carbonyl Q° moment in leading to CD. In addition, the transition energy at which this background CD appears [it has been suggested that amide and acidic carbonyls have their n → π* transitions at ~260 nm (in alcohols)[22]] coincides more with that of the L_b band, and thus the carbonyl CD is unlikely to effect the analysis of the selected probe transitions.

Comparisons with Experimental Data

All the crowns **1–5** have strong CD bands at the L_a and n transitions (see Figures 5 and 6). In all cases, the L_a band is negative in sign, and its sharp slope at higher energy is consistent with the appearance of a "partner" exciton band corresponding to the amide carbonyl. This is fully consistent with the theoretical prediction of the previous section (see eq 30 for the relevant CD spectrum–structure relationship) that the L_a CD will be strongly negative for the experimentally determined basis structure in which the amide carbonyl is found to have (for the reference to the right) $\xi = 30°$, with the other being related by the C_2 axis of the pyridyl and thus contributing constructively.

In addition, all the crowns have an n band that is negative. Noting that all spectra are determined in alcohol, a highly polarizable solvent, this is consistent with the theoretical predictions assuming a dominant contribution from the crown holes (filled with solvent), which lie exclusively in the quadrants that contribute a negative CD (see eq 36 for the relevant CD spectrum–structure relationship). In a sense, the R groups in this case serve to exclude potentially cancelling positive contributions from the solvent if the system was achiral, and thus the CD should increase as the size of the R group increases. This general behavior is found experimentally for the series **1–3**.

The exceptional case here is the inverted crown **4**, which should have, if it has a structure similar to the basis structure, a positive n CD and a negative L_a CD. Experimentally, both bands are negative. However, the conformation of the basis structure is partially controlled by H–H repulsions between the amide hydrogens and the CH of the pyridyl group in the AC system, whereas the inverted system presents the pyridyl lone pairs and leads to the potential formation of hydrogen bonds with the amide hydrogens. In such a case, the GSR/ISP expressions for the n-transition CD must be augmented by overlap-dependent dative terms.[23] A preliminary analysis of such additive dative terms suggests a strong negative dative CD contribution for the basis structure geometry, thereby leading to the overall negative n CD for the inverted crown **4**, as observed experimentally. A detailed discussion of this dative mechanism will be published elsewhere. Supporting evidence that such an extra mechanism occurs for the particular crown **4** is supported by the inverted crowns studied by Dyer et al.,[2] for which dativity (hydrogen bonding) is absent. If we assume that their structures are consistent with that of the basis structure, the theoretical expectation of a positive n band and negative L_a band for the inverted complexes is confirmed.

Conclusions

The present analysis for the pyridine crowns suggests that the CD of the pyridine n transition is, in these compounds, a sensitive extrinsic probe of the crown holes, and thus of the nature of the chemical moities present therein. This is a particularly encouraging result as it is, after all, precisely such intercalation processes that are crucial to the practical importance of such crown systems. The CD of the L_a transition, on the other hand, serves as an intrinsic structural probe of the crown backbone. Thus, pyridine is a particularly suitable probe in that it is capable of monitoring, through its two distinct probe transitions, two different aspects of the crown structure.

(23) Schipper, P. E. *Recl. Trav. Chim. Pays-Bas*, in press.

Vibrational Optical Activity in *trans*-2,3-Dimethyloxirane

Thomas M. Black,[†] Pranati K. Bose,[†] Prasad L. Polavarapu,*[,†] Laurence D. Barron,*[,‡] and Lutz Hecht[‡]

Contribution from the Departments of Chemistry, Vanderbilt University, Nashville, Tennessee 37235, and The University, Glasgow G128QQ, UK. *Received June 14, 1989*

Abstract: Vibrational circular dichroism (VCD) and Raman optical activity (ROA) spectra for *trans*-2,3-dimethyloxirane are presented. Ab initio vibrational properties obtained with the 6-31G, 6-311G, and 6-31G** basis sets are used to understand the nature of vibrations responsible for the observed bands. On the basis of these vibrational assignments VCD spectral features were interpreted by using the VCD expressions derived for A_2B_2 molecules of C_2 symmetry. The absolute configuration deduced from these VCD interpretations matches that known from other experiments. Recent instrumental developments permitted the measurements of the first ROA spectra in backward scattering for *trans*-2,3-dimethyloxirane. These experimental ROA spectra were analyzed by using the ab initio ROA predictions obtained with the 6-31G and 6-31G** basis sets. For the majority of vibrational bands the predicted ROA signs are in agreement with the observed ones. However, the predicted ROA magnitudes, normalized with the Raman intensities, are usually larger than the experimental magnitudes.

I. Introduction

Vibrational Raman optical activity[1] (ROA) and circular dichroism[2] (VCD) are two new branches of molecular spectroscopy that probe the optical activity associated with vibrational transitions. The major anticipation of vibrational optical activity (VOA) is to provide new approaches for determining the three-

[†] Vanderbilt University.
[‡] The University.

(1) (a) Barron, L. D.; Buckingham, A. D. *Mol. Phys.* **1971**, *20*, 1111–1119. (b) Barron, L. D.; Bogaard, M. P.; Buckingham, A. D. *J. Am. Chem. Soc.* **1973**, *95*, 603.

0002-7863/90/1512-1479$02.50/0

Table I. Cartesian Coordinates (Å) for the Optimum Geometry of *trans*-(2*R*,3*R*)-Dimethyloxirane

		6-31G basis set			6-311G basis set			6-31G** basis set		
no.	atom	*x*	*y*	*z*	*x*	*y*	*z*	*x*	*y*	*z*
1	O	0.0000	0.0000	0.0000	0.0000	0.0000	0.0000	0.0000	0.0000	0.0000
2	C	0.0000	0.0000	1.4654	0.0000	0.0000	1.4586	0.0000	0.0000	1.4076
3	C	1.2690	0.0000	0.7328	1.2665	0.0000	0.7235	1.2450	0.0000	0.6569
4	H	1.7892	0.9364	0.6548	1.7825	0.9362	0.6457	1.7738	0.9389	0.5744
5	C	2.1137	−1.2287	0.5764	2.1127	−1.2253	0.5661	2.0947	−1.2292	0.4810
6	H	−0.3277	−0.9364	1.8769	−0.3235	−0.9362	1.8681	−0.3197	−0.9389	1.8368
7	C	−0.5578	1.2287	2.1187	−0.5563	1.2253	2.1153	−0.5520	1.2292	2.0772
8	H	−0.1822	2.1235	1.6390	−0.1934	2.1191	1.6286	−0.1920	2.1266	1.5871
9	H	−0.2879	1.2594	3.1687	−0.2709	1.2625	3.1596	−0.2581	1.2598	3.1222
10	H	−1.6388	1.2404	2.0468	−1.6366	1.2302	2.0591	−1.6364	1.2302	2.0305
11	H	1.5104	−2.1235	0.6619	1.5100	−2.1191	0.6399	1.4933	−2.1266	0.5708
12	H	2.8880	−1.2594	1.3352	2.8779	−1.2625	1.3320	2.8819	−1.2598	1.2287
13	H	2.5920	−1.2404	−0.3956	2.5997	−1.2302	−0.3997	2.5595	−1.2302	−0.4998

dimensional structure of chiral molecules in the solution phase. To reach this goal, simple theoretical models applicable to localized vibrations associated with certain segments in a molecule possessing local symmetry or to the degeneracy-lifted vibrations of a symmetric group in a chiral environment have been developed.[3-8] In practice it is usually difficult to verify these models because either the desired vibrational bands cannot be identified unambiguously or the molecule under investigation does not have the necessary local symmetry. Despite these difficulties much progress has been made in recent years and a few examples are now available where VOA has been shown[9] to independently provide configurational or conformational information.

trans-2,3-Dimethyloxirane is of special interest in this context for the following reasons: (a) Due to the presence of C_2 symmetry, VOA associated with the vibrations of H–C*–C*–H and C–C*–C*–C segments provide a direct experimental verification of the utility of simple theoretical models. (b) The size of this molecule is appropriate for a reliable ab initio vibrational analysis, and the desired vibrational bands can be identified with the help of ab initio calculations. The depolarized ROA associated with the methyl torsion vibration of (−)-*trans*-(2*S*,3*S*)-dimethyloxirane has been discussed earlier.[10] More recently, the polarized and depolarized ROA associated with the ring C–O stretching vibrations have been discussed.[11] The VCD spectra however have not been reported to date.

For interpreting the optical activity associated with the vibrational transitions, a reliable vibrational analysis is necessary. Durig and co-workers[12] reported the vibrational spectra of *trans*-2,3-dimethyloxirane and suggested tentative vibrational assignments. The recent development of sophisticated ab initio programs[13,14] permits detailed vibrational calculations, so that the VOA spectra can be interpreted confidently. In addition, by evaluating the electric dipole–magnetic dipole and electric dipole–electric quadrupole polarizabilities at displaced geometries it is now possible to determine the ab initio ROA spectra.[15,16] The theoretical ROA signs obtained in this way were found to be in agreement with the experimental observations for most of the vibrations of methylthiirane[15] and methyloxirane.[16] Similar ab initio ROA investigations on *trans*-2,3-dimethyloxirane are of special interest as the experimental ROA spectra were found to suggest some unusual electronic effects.[11]

In this paper we report and discuss (a) VCD spectra in the 1600–700 cm^{-1} region, (b) depolarized, polarized, and backscattered ROA spectra in the 1600–100 cm^{-1} region, (c) ab initio vibrational analysis and infrared and Raman intensities using 6-31G, 6-311G, and 6-31G** basis sets, and (d) ab initio ROA calculations with 6-31G and 6-31G** basis sets.

II. Experimental and Computational Details

The VCD spectra in the 1600–700 cm^{-1} region were measured on a VCD instrument that was recently assembled at Vanderbilt by modifying a CYGNUS-100 (Mattson Instruments) FTIR spectrometer. The measurement procedure is similar to that described in our earlier measurements.[17] A higher sensitivity liquid nitrogen cooled HgCdTe detector ($D^* = 6 \times 10^{10}$, 1 mm^2 area, 650 cm^{-1} cut-off) was used for the spectra presented here. The VCD spectra were measured at 4 cm^{-1} resolution for both enantiomers of *trans*-2,3-dimethyloxirane in CCl_4 and CS_2 solutions. The raw VCD of the racemic mixture is subtracted from those of the individual enantiomers to suppress the base line artifacts. The ROA spectra were measured on a multichannel Raman spectrometer[18] assembled at Glasgow. The neat liquid sample was distilled into a micro quartz fluorescence cell and ROA spectra were obtained with the use of a focussed 600 mW argon ion laser beam at 488 nm with an effective spectral slit width (fwhh) of 6 cm^{-1}. The single channel depolarized ROA spectrum reported earlier[10] was remeasured together with polarized and backscattered[19] ROA spectra.

Geometry optimization, vibrational frequency, and vibrational intensity calculations were carried out with 6-31G, 6-311G, and 6-31G** basis sets with the GAUSSIAN 86[13] and CADPAC[14] programs. For the purpose of ab initio calculations, Placzek's approximation was invoked to write the depolarized (z) and polarized (x)[1,4] ROA intensities for scattering in the

(2) (a) Holzwarth, G.; Hsu, E. C.; Mosher, H. S.; Faulkner, T. R.; Moscowitz, A. *J. Am. Chem. Soc.* **1974**, *96*, 251–252. (b) Nafie, L. A.; Keiderling, T. A.; Stephens, P. J. *J. Am. Chem. Soc.* **1976**, *98*, 2715–2723.

(3) (a) Holzwarth, G.; Chabay, I. *J. Chem. Phys.* **1972**, *57*, 1632–1635. (b) Schellman, J. *J. Chem. Phys.* **1973**, *58*, 2882–2886.

(4) (a) Barron, L. D. In *Optical Activity and Chiral Discrimination*; Mason, S. F., Ed.; Reidel: Dordrecht, 1979. (b) Barron, L. D. *Molecular Light Scattering and Optical Activity*; Cambridge University Press: Cambridge, 1982.

(5) Polavarapu, P. L. *J. Chem. Phys.* **1987**, *87*, 4419–4422; **1986**, *85*, 6245–6246.

(6) Gohin, A.; Moskovits, M. *J. Am. Chem. Soc.* **1981**, *103*, 1660–1664.

(7) (a) Barron, L. D. *Nature* **1975**, *255*, 458–460. (b) Hug, W.; Kint, S.; Bailey, G. F.; Scherer, J. R. *J. Am. Chem. Soc.* **1975**, *97*, 5590–5591.

(8) Nafie, L. A.; Polavarapu, P. L.; Diem, M. *J. Chem. Phys.* **1980**, *73*, 3530–3540.

(9) (a) Freedman, T. B.; Paterlini, M. G.; Lee, N.; Nafie, L. A.; Schwab, J. M.; Ray, T. *J. Am. Chem. Soc.* **1987**, *109*, 4727–4728. (b) Polavarapu, P. L.; Ewig, C. S.; Chandramouly, T. *J. Am. Chem. Soc.* **1987**, *109*, 7382–7386. (c) Su, C. N.; Keiderling, T. A. *J. Am. Chem. Soc.* **1980**, *102*, 511–515.

(10) Barron, L. D.; Vrbancich, J. *Mol. Phys.* **1983**, *48*, 833–845.

(11) Barron, L. D.; Polavarapu, P. L. *Mol. Phys.* **1988**, *65*, 659–667.

(12) Durig, J. R.; Nease, A. B.; Rizzolo, J. J. *J. Mol. Struct.* **1982**, *95*, 59–84.

(13) Frisch, M. J.; Binkley, J. S.; Schlegel, H. B.; Raghavachari, K.; Melius, C.; Martin, R. L.; Stewart, J. J. P.; Bobrowicz, F. W.; Rohlfing, C. M.; Kahn, R. L.; Defrees, D. J.; Seeger, R.; Whiteside, R. A.; Fox, D. J.; Fleuder, E. M.; Pople, J. A. *GAUSSIAN 86*; Carnegie-Mellon Quantum Chemistry Publishing Unit: Pittsburgh, PA, 1986.

(14) Amos, R. D.; Rice, J. E. *CADPAC*; The Cambridge Analytic Derivatives Package: Cambridge, 1987; Issue 4.0.

(15) Bose, P. K.; Barron, L. D.; Polavarapu, P. L. *Chem. Phys. Lett.* **1989**, *155*, 423–429.

(16) Bose, P. K.; Polavarapu, P. L.; Barron, L. D.; Hecht, L. *J. Phys. Chem.*, in press.

(17) Polavarapu, P. L. In *Fourier Transform Infrared Spectroscopy*; Ferraro, J. R., Basile, L. J., Eds.; Academic Press: New York, 1985; Vol. 4, pp 61–96.

(18) Barron, L. D.; Cutler, D. J.; Torrance, J. F. *J. Raman Spectrosc.* **1987**, *18*, 281–287.

(19) Hecht, L.; Barron, L. D.; Hug, W. *Chem. Phys. Lett.* **1989**, *158*, 341–344.

Table II. Force Constants Providing Major Potential Energy Contributions[a] to the ab Initio Normal Modes in *trans*-2,3-Dimethyloxirane

6-31G basis set		6-31G** basis set	
freq	major PE contributor	freq	major PE contributor
1661	F_3, F_{16}, F_{17}	1682	F_3, F_{16}, F_{17}
1652	F_{33}, F_{30}, $F_{31,33}$, $F_{28,30}$, F_{31}, F_{28}	1623	F_{33}, F_{30}, $F_{31,33}$, $F_{28,30}$
1649	F_{28}, F_{31}, $F_{28,30}$, $F_{31,33}$	1620	F_{28}, F_{31}, $F_{28,30}$, $F_{31,33}$, F_{30}, F_{33}
1640	F_{32}, F_{29}, $F_{28,29}$, $F_{31,32}$, F_{28}, F_{31}	1610	F_{31}, F_{28}, F_{32}, F_{29}, $F_{31,32}$, $F_{28,29}$
1622	F_{17}, F_{16}, F_3, F_{29}, F_{32}	1606	F_{29}, F_{32}, $F_{28,29}$, $F_{31,32}$, $F_{29,30}$, $F_{32,33}$
1588	F_{23}, F_{26}, F_{22}, F_{25}, F_{24}, F_{27}	1556	F_{25}, F_{22}, F_{26}, F_{23}, F_{27}, F_{24}
1587	F_{26}, F_{23}, F_{27}, F_{24}, F_{25}, F_{22}	1546	F_{23}, F_{26}, F_{24}, F_{27}, F_{22}, F_{25}
1505	F_{16}, F_{17}, F_{15}, F_{14}	1493	F_{15}, F_{14}, F_{16}, F_{17}
1391	F_3, F_{15}, F_{14}, F_{17}, F_{16}	1400	F_{14}, F_{15}, F_3, F_{17}, F_{16}
1319	F_{33}, F_{30}, $F_{31,33}$, $F_{28,30}$, $F_{32,33}$, $F_{29,30}$	1325	F_{30}, F_{33}, $F_{29,30}$, $F_{32,33}$, F_{29}, F_{32}
1307	F_{29}, F_{32}, $F_{29,30}$, $F_{32,33}$, F_{30}, F_{33}	1302	F_{32}, F_{29}, $F_{32,33}$, $F_{29,30}$, $F_{31,32}$, $F_{28,29}$
1261	F_{32}, F_{29}, F_{27}, F_{24}, $F_{32,33}$, $F_{29,30}$	1250	F_{25}, F_{22}, F_{24}, F_{27}, F_{29}, F_{32}
1240	F_{23}, F_{26}, F_5, F_{10}, F_{25}, F_{22}	1218	F_{26}, F_{23}, F_{10}, F_5, F_{30}, F_{33}
1154	F_{31}, F_{28}, $F_{31,32}$, $F_{28,29}$, F_{23}, F_{26}	1141	F_{10}, F_5, F_2, F_1, F_{26}, F_{23}
1138	F_{10}, F_5	1141	F_{28}, F_{31}, $F_{28,29}$, $F_{31,32}$, F_{32}, F_{29}
1091	F_{28}, F_{31}, $F_{28,30}$, $F_{31,33}$, F_{24}, F_{27}	1055	F_{28}, F_{31}, F_{24}, F_{27}, $F_{28,30}$, $F_{31,33}$
956	F_{10}, F_5, F_2, F_1, F_{25}, F_{22}	1003	F_2, F_1, F_{23}, F_{26}
866	F_3, F_2, F_1	893	F_3
787	F_1, F_2	854	F_1, F_2
499	F_{20}, F_{18}	516	F_{18}, F_{20}
498	F_{21}, F_{19}	490	F_{19}, F_{21}, F_{20}, F_{18}
308	F_{19}, F_{21}	302	F_{19}, F_{21}, F_{32}, F_{29}
266	F_{28}, F_{31}, $F_{31,32}$, $F_{28,29}$, $F_{31,33}$, $F_{28,30}$	267	F_{31}, F_{28}, $F_{31,32}$, $F_{28,29}$, $F_{31,33}$, $F_{28,30}$
211	methyl torsion	224	methyl torsion
193	methyl torsion	203	methyl torsion

[a] There is some arbitrariness in limiting the number of force constants that appear in this table. The criterion used is that those force constants which provide potential energy contributions that are approximately within 50% of the most dominant contribution are considered, but the total number is limited to six. The force constants are listed in the decreasing order of their contributions. F_i represents the force constant associated with ith internal coordinate and $F_{i,j}$ represents the interaction force constant associated with i and j.

90° direction together with that for backscattering (180°),[4b,19] expressed as the normalized circular intensity difference (CID), in the form

$$\Delta_z = \left(\frac{2\pi}{\lambda}\right)\frac{4\left(\frac{3}{\omega}\frac{\partial\alpha_{\alpha\beta}}{\partial Q_i}\frac{\partial G'_{\alpha\beta}}{\partial Q_i} - \frac{1}{\omega}\frac{\partial\alpha_{\alpha\alpha}}{\partial Q_i}\frac{\partial G'_{\beta\beta}}{\partial Q_i} - \frac{1}{3}\epsilon_{\alpha\gamma\delta}\frac{\partial\alpha_{\alpha\beta}}{\partial Q_i}\frac{\partial A_{\gamma\delta\beta}}{\partial Q_i}\right)}{2\left(3\frac{\partial\alpha_{\lambda\mu}}{\partial Q_i}\frac{\partial\alpha_{\lambda u}}{\partial Q_i} - \frac{\partial\alpha_{\lambda\lambda}}{\partial Q_i}\frac{\partial\alpha_{\mu\mu}}{\partial Q_i}\right)} \quad (1)$$

$$\Delta_x = \left(\frac{2\pi}{\lambda}\right)\frac{2\left(\frac{7}{\omega}\frac{\partial\alpha_{\alpha\beta}}{\partial Q_i}\frac{\partial G'_{\alpha\beta}}{\partial Q_i} + \frac{1}{\omega}\frac{\partial\alpha_{\alpha\alpha}}{\partial Q_i}\frac{\partial G'_{\beta\beta}}{\partial Q_i} + \frac{1}{3}\epsilon_{\alpha\gamma\delta}\frac{\partial\alpha_{\alpha\beta}}{\partial Q_i}\frac{\partial A_{\gamma\delta\beta}}{\partial Q_i}\right)}{\left(7\frac{\partial\alpha_{\lambda\mu}}{\partial Q_i}\frac{\partial\alpha_{\lambda\mu}}{\partial Q_i} + \frac{\partial\alpha_{\lambda\lambda}}{\partial Q_i}\frac{\partial\alpha_{\mu\mu}}{\partial Q_i}\right)} \quad (2)$$

$$\Delta(180°) = \left(\frac{2\pi}{\lambda}\right)\frac{8\left(\frac{3}{\omega}\frac{\partial\alpha_{\alpha\beta}}{\partial Q_i}\frac{\partial G'_{\alpha\beta}}{\partial Q_i} - \frac{1}{\omega}\frac{\partial\alpha_{\alpha\alpha}}{\partial Q_i}\frac{\partial G'_{\beta\beta}}{\partial Q_i} + \frac{1}{3}\epsilon_{\alpha\gamma\delta}\frac{\partial\alpha_{\alpha\beta}}{\partial Q_i}\frac{\partial A_{\gamma\delta\beta}}{\partial Q_i}\right)}{\left(7\frac{\partial\alpha_{\lambda\mu}}{\partial Q_i}\frac{\partial\alpha_{\lambda\mu}}{\partial Q_i} + \frac{\partial\alpha_{\lambda\lambda}}{\partial Q_i}\frac{\partial\alpha_{\mu\mu}}{\partial Q_i}\right)} \quad (3)$$

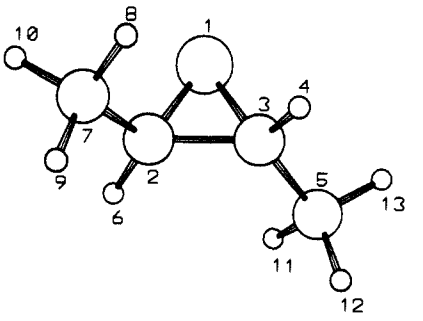

Figure 1. Atomic numbering for *trans*-(2*R*,3*R*)-dimethyloxirane.

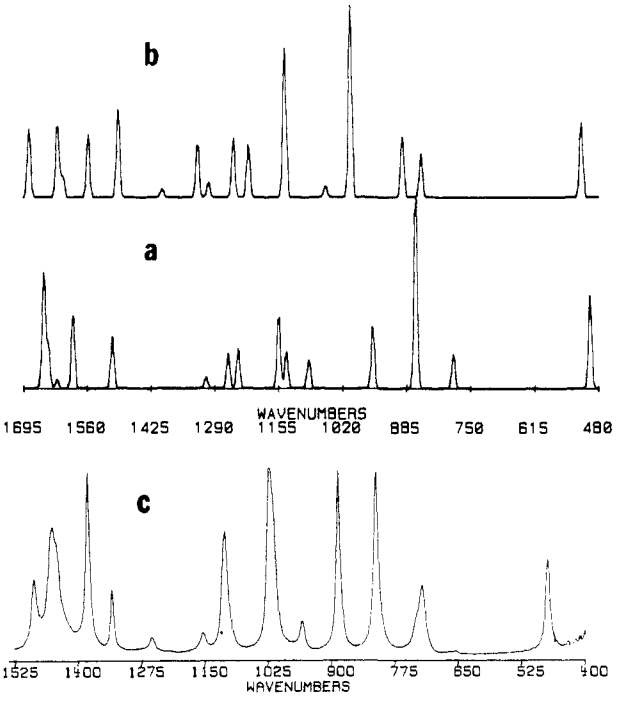

Figure 2. Ab initio and experimental infrared absorption spectra of *trans*-2,3-dimethyloxirane. The theoretical spectra were obtained with the 6-31G (a) and 6-31G** (b) basis sets. The experimental spectrum (c) was obtained for the neat liquid.

Table III. Internal Coordinates[a] Used for Force Constant Calculations

coordinate	definition	coordinate	definition	coordinate	definition
R_1	$r_{1,2}$	R_{12}	$r_{7,9}$	R_{23}	$\alpha_{9,7,2}$
R_2	$r_{1,3}$	R_{13}	$r_{7,10}$	R_{24}	$\alpha_{10,7,2}$
R_3	$r_{2,3}$	R_{14}	$\alpha_{1,3,4}$	R_{25}	$\alpha_{11,5,3}$
R_4	$r_{3,4}$	R_{15}	$\alpha_{1,2,6}$	R_{26}	$\alpha_{12,5,3}$
R_5	$r_{3,5}$	R_{16}	$\alpha_{3,2,6}$	R_{27}	$\alpha_{13,5,3}$
R_6	$r_{5,11}$	R_{17}	$\alpha_{2,3,4}$	R_{28}	$\tau_{8,7,2,6}$
R_7	$r_{5,12}$	R_{18}	$\alpha_{1,3,5}$	R_{29}	$\tau_{9,7,2,6}$
R_8	$r_{5,13}$	R_{19}	$\alpha_{2,3,5}$	R_{30}	$\tau_{10,7,2,6}$
R_9	$r_{2,6}$	R_{20}	$\alpha_{1,2,7}$	R_{31}	$\tau_{11,5,3,4}$
R_{10}	$r_{2,7}$	R_{21}	$\alpha_{3,2,7}$	R_{32}	$\tau_{12,5,3,4}$
R_{11}	$r_{7,8}$	R_{22}	$\alpha_{8,7,2}$	R_{33}	$\tau_{13,5,3,4}$

[a] $r_{1,2}$ for example is the distance between atoms 1 and 2; $\alpha_{1,3,4}$ is the angle made by atoms 1, 3, and 4; $\tau_{8,7,2,6}$ is the dihedral angle between the planes of atoms 8, 7, and 2 and of 7, 2, and 6. The numbering of atoms and their coordinates are given in Table I.

where $\Delta_\alpha = (I_\alpha^R - I_\alpha^L)/(I_\alpha^R + I_\alpha^L)$, with I_α^R and I_α^L representing the Raman scattered intensities for right and left circularly polarized incident light, in 90° scattering (α = z or x) or backward scattering (α = 180°) geometry; $\alpha_{\alpha\beta}$ is the electric dipole–electric dipole polarizability, $G'_{\alpha\beta}$ is the electric dipole–magnetic dipole polarizability, $A_{\alpha\beta\gamma}$ is the electric dipole–electric quadrupole polarizability, Q_i is the ith vibrational normal coordinate, and λ is the exciting wavelength with an associated angular frequency ω. The gradients required in eqs 1–3 were obtained numerically by evaluating the tensors $\alpha_{\alpha\beta}$, $\omega^{-1}G'_{\alpha\beta}$, and $A_{\alpha\beta\gamma}$ at the optimized geometry and by displacing each atomic coordinate by 0.005 Å. The

Table IV. Ab Initio Vibrational Intensities[a] for *trans*-(2*R*,3*R*)-Dimethyloxirane

	6-31G basis set				6-311G basis set				6-31G** basis set			
		intensities				intensities				intensities		
			Raman				Raman				Raman	
	freq, cm^{-1}	IR	$45\bar{\alpha}^2 + 4\beta(\alpha)^2$	$3\beta(\alpha)^2$	freq, cm^{-1}	IR	$45\bar{\alpha}^2 + 4\beta(\alpha)^2$	$3\beta(\alpha)^2$	freq, cm^{-1}	IR	$45\bar{\alpha}^2 + 4\beta(\alpha)^2$	$3\beta(\alpha)^2$
A	1661	0.24	7.64	5.47	1659	1.49	3.56	2.26	1682	12.70	1.89	0.30
B	1652	8.45	12.45	9.34	1647	7.64	10.16	7.62	1623	5.88	9.34	7.01
A	1649	16.36	3.25	2.42	1643	16.69	3.06	2.26	1620	8.65	5.25	3.93
B	1640	7.99	12.09	9.07	1634	9.26	8.73	6.55	1610	3.66	10.34	7.75
A	1622	1.83	9.92	6.22	1621	1.54	9.05	5.88	1606	0.41	10.05	7.14
B	1588	14.60	1.24	0.93	1579	15.22	0.86	0.64	1556	11.74	0.97	0.73
A	1587	0.47	2.79	2.04	1576	0.13	1.74	1.24	1546	0.00	1.74	1.26
B	1505	10.78	0.67	0.50	1498	11.68	0.65	0.49	1493	16.10	0.92	0.69
A	1391	0.14	14.23	5.75	1392	0.38	14.15	5.12	1400	1.61	13.09	4.73
A	1319	0.09	2.78	0.35	1316	0.79	2.63	0.30	1325	10.03	1.80	0.39
B	1307	2.26	2.44	1.83	1310	2.08	2.15	1.62	1302	2.67	2.38	1.79
A	1261	7.30	3.40	2.55	1257	9.05	2.85	2.12	1250	11.09	2.90	1.65
B	1240	8.01	1.38	1.03	1235	8.80	1.01	0.76	1218	9.84	0.54	0.41
A	1154	14.63	1.65	0.42	1151	12.89	1.45	0.38	1141	15.37	2.09	0.95
B	1138	7.21	2.14	1.60	1143	8.82	2.07	1.55	1141	12.39	1.71	1.28
B	1091	5.87	3.57	2.68	1085	4.28	2.80	2.10	1055	2.11	2.45	1.84
A	956	12.71	14.84	1.86	958	18.47	13.57	1.75	893	11.26	10.52	4.23
A	866	38.26	6.35	4.75	870	42.66	6.23	4.54	1003	35.54	4.87	1.65
B	787	6.77	9.76	7.32	804	7.04	8.96	6.72	854	8.14	5.75	4.31
B	499	18.46	0.34	0.26	503	18.81	0.26	0.19	516	13.75	0.05	0.04
A	498	0.01	4.11	0.94	496	0.01	3.85	0.79	490	0.01	3.30	0.67
B	308	0.96	0.24	0.18	306	0.96	0.20	0.15	302	0.94	0.27	0.21
A	266	2.50	0.09	0.06	268	2.27	0.09	0.07	267	1.72	0.08	0.05
B	211	0.66	0.03	0.02	214	0.57	0.02	0.02	224	0.48	0.02	0.02
A	193	0.25	0.07	0.05	195	0.25	0.13	0.09	203	0.31	0.07	0.05

[a] IR intensities are in km/mol and Raman intensities are in (Å⁴/amu). $\bar{\alpha}$ is the mean of the normal coordinate derivative of the polarizability tensor; $\beta(\alpha)^2$ is the anisotropy of that tensor.

procedure for evaluating these tensors is due to Amos,[20] as implemented in the CADPAC program.[14] The calculations were done with the origin at the O atom and at the center of the charge of the nuclei. The CIDs were evaluated for the exciting wavelength of 488 nm used in the experiment. The theoretical spectra were simulated with a 5 cm^{-1} bandwidth.

III. Results and Discussion

A. Vibrational Analysis. The geometries optimized with 6-31G, 6-311G, and 6-31G** basis sets are presented in Table I. The atomic numbering for *trans*-(2*R*,3*R*)-dimethyloxirane is shown in Figure 1. In order to facilitate the discussion of band assignments obtained with these different basis sets the particular internal coordinate force constants, which provide the major potential energy contribution to a given normal mode, are determined (Table II). The internal coordinate definitions employed for this purpose are summarized in Table III. The potential energy contribution from the individual force constants obtained with the 6-31G and 6-311G basis sets differ insignificantly. For this reason the mode assignments derived from the 6-311G basis set calculations will not be specifically referred to in the discussion. The ab initio vibrational intensities are summarized in Table IV. The discussion in this paper is limited to the experimental bands in the ~1600–100 cm^{-1} region.

In the 1500–1400 cm^{-1} region, the experimental infrared spectrum (Figure 2) contains one isolated band at 1489 cm^{-1} and a set of overlapping bands with absorption maximum at 1452 cm^{-1}. This 1452 cm^{-1} band exhibits a shoulder on the lower frequency side. The experimental Raman spectrum (Figure 3) contains one band at 1487 cm^{-1} and two bands at ~1445 and 1426 cm^{-1}. In the ab initio predictions the highest frequency mode (namely the 6-31G mode at 1661 cm^{-1}, the 6-311G mode at 1659 cm^{-1}, and the 6-31G** mode at 1682 cm^{-1}) belonging to the A irreducible representation has major potential energy contributions from the H–C*–C* bending and C*–C* stretching force constants. Therefore, we assign the experimental infrared band at 1489 cm^{-1} and the Raman band at ~1487 cm^{-1} to the symmetric combination of the two H–C*–C* bending motions. Following similar guidelines from the ab initio calculations, the overlapping infrared bands at ~1452 cm^{-1} and the Raman bands at ~1445 and 1426 cm^{-1} are associated with four methyl bending modes (see Table V). These arise from the antisymmetric and symmetric combinations of the near-degenerate methyl antisymmetric deformations from the two individual methyl groups. The 6-31G frequencies, for example, of these modes are 1652, 1649, 1640,

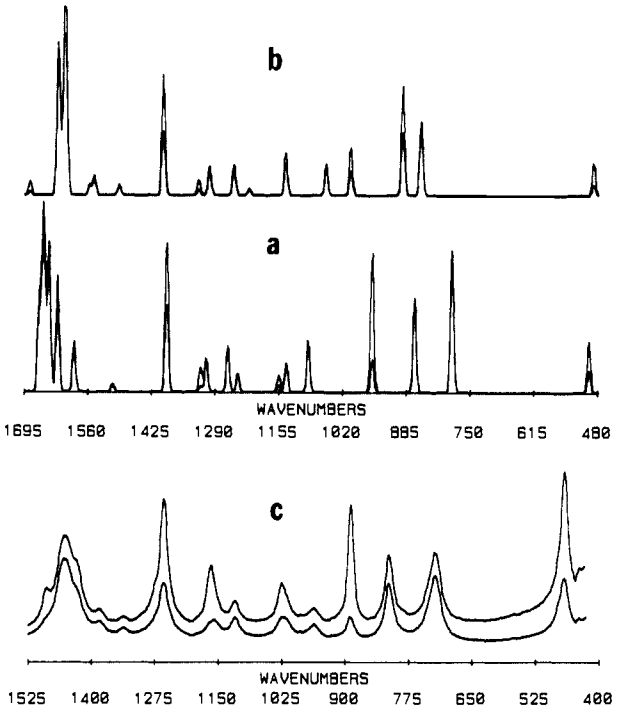

Figure 3. Ab initio and experimental Raman spectra of *trans*-2,3-dimethyloxirane. The theoretical spectra were obtained with the 6-31G (a) and 6-31G** (b) basis sets. The experimental spectra (c) were obtained for the neat liquid in the 90° scattering geometry. The two traces for each case represent polarized (top) and depolarized (bottom) spectra and are proportional to $(\nu_0 - \nu)^4(45\bar{\alpha}^2 + 7\beta(\alpha)^2)$ and $(\nu_0 - \nu)^4 \cdot (6\beta(\alpha)^2)$, respectively.

(20) Amos, R. D. *Chem. Phys. Lett.* **1982**, *87*, 23–26.

Table V. Vibrational Frequencies and Assignments for *trans*-2,3-Dimethyloxirane

present work							ref 12		
theoretical			experimental						
symmetry	6-31G	6-311G	6-31G**	IR	Raman	group assignment[a]	symmetry	frequency	assignment
A	1661	1659	1682	1489	1487	H–C*–C*, C*–C*	A	1488	CH_3
B	1652	1647	1623	1452		CH_3	B	1475	CH_3
A	1649	1643	1620	1452		CH_3	B	1462	CH_3
B	1640	1634	1610		1445	CH_3	A	1440	CH_3
A	1622	1621	1606		1426	CH_3, H–C*–C*	A	1425	CH_3
B	1588	1579	1556	1381	1381	CH_3	B	1385	CH_3
A	1587	1576	1546	1381	1381	CH_3			
B	1505	1498	1493	1335	1335	H–C*–C*, H–C*–O	B	1336	C–H bend
							A	1275	C–H bend
A	1391	1392	1400	1254	1254	C*–C*, H–C*–O, H–C*–C*	A	1255	ring breathing
A	1319	1316	1325		1163	CH_3–C*–H	A	1167	C–H bend
B	1307	1310	1302	1154		CH_3–C*–H			
A	1261	1257	1250	1110	1113	CH_3–C*–H	B	1117	C–H bend
B	1240	1235	1218	1110	1113	CH_3, C–C*	B	1109	CH_3 rock
							A	1031	CH_3 rock
A	1154	1151	1141	1015		CH_3–C*–H	A	1023	CH_3 rock
B	1138	1143	1141	1022	1022	C*–C	B	1020	CH_3 rock
B	1091	1085	1055	959	960	CH_3–C*–H	B	957	C–C
A	956	958	893[b]	886	886	C*–C	A	893	ring def
A	866	870	1003[b]	812	811	C*–O	A	813	C–C
B	787	804	854	722	719	C*–O	B	735	ring def
B	499	503	516	473	473	C–C*–O	B	471	skeletal bend
A	498	496	490		466	C–C*–C*	A	469	skeletal bend
B	308	306	302		289	C–C*–C*	B	289	skeletal bend
A	266	268	267		249	CH_3–C*–H	A	249	skeletal bend
B	211	214	224		200	torsion	B	200	torsion
A	193	195	203		185	torsion	A	181	torsion

[a] Derived from 6-31G and calculations. [b] Frequency order of these two bands is interchanged as discussed in the text.

and 1622 cm^{-1}. Since the associated bands are not resolved in the infrared spectrum, there remains an uncertainty in verifying the predicted frequency order of these four modes. Nevertheless, the experimental Raman bands at ~1445 and 1426 cm^{-1} are better resolved and therefore the associated ROA signs provide a basis for verifying the predicted frequency ordering. From the experimental and ab initio ROA signs (vide infra) the predicted frequency ordering of these four modes appears to be reliable.

The vibrational frequency of the H–C*–C* bending mode discussed in the previous paragraph appears to depend on the nature of the heteroatom in the ring and on that of substituents at the chiral center. From our own ab initio calculations on 1,2-dideuteriocyclopropane and 1,2-dideuteriooxirane, the symmetric methine bending mode corresponds to the experimental[21] band at 1355 cm^{-1} in the former and at 1397 cm^{-1} in the latter. It is possible that the presence of methyl groups at the chiral centers in *trans*-2,3-dimethyloxirane shifted the frequency of the symmetric H–C*–C* bending mode to a higher value compared to that in 1,2-dideuteriooxirane. In the absence of isotopic substitution data for *trans*-2,3-dimethyloxirane one cannot confirm the present assignment for the 1487 cm^{-1} Raman band, but the agreement between the calculated and observed ROA for this band (vide infra) supports the present assignment.

The symmetric and antisymmetric combinations of the umbrella type bending motions of individual methyl groups are predicted to be nearly degenerate with the 6-31G frequencies of 1588 and 1587 cm^{-1}. The corresponding 6-311G and 6-31G** frequencies are 1579 and 1576 cm^{-1} and 1556 and 1546 cm^{-1}, respectively. One of these two modes belonging to the **B** irreducible representation is predicted to have large infrared absorption, while the other is predicted to have only a very small absorption (Table IV), suggesting that only one absorption band could be observed in the infrared spectrum. Although these two modes are predicted to have Raman intensities of roughly the same magnitude (Table IV), the small frequency difference predicted by the 6-31G and 6-311G basis sets suggests that both components may not be resolved in the experimental Raman spectrum. The 6-31G** calculations predict a 10 cm^{-1} difference for the frequencies of these modes, but we do not see two Raman bands at this separation in the experimental spectrum. Therefore we assign the 1381 cm^{-1} band in the experimental spectra to both CH_3 modes, as discussed in this paragraph, with infrared absorption mostly due to the **B** mode and Raman intensity due to both **A** and **B** modes. One could conceivably associate the experimental Raman bands at 1426 and 1381 cm^{-1} or those at 1381 and 1335 cm^{-1} with the two modes under discussion, but that would mean a ~45 cm^{-1} frequency difference for these modes which is difficult to explain.

The next lower frequency band at ~1335 cm^{-1} is assigned to the antisymmetric combination of the methine bending motions, based on the observation that the calculations predict the corresponding theoretical mode (namely the 6-31G mode at 1505 cm^{-1} and the 6-31G** mode at 1492 cm^{-1}) to have a major potential energy contribution from the H–C*–C* and H–C*–O bending force constants. All calculations predict relatively strong infrared absorption and weak Raman intensity for this mode which is qualitatively in agreement with the experimental observations. However, one point worth mentioning is that the 6-31G** calculations predict more absorption intensity for this mode than for the two CH_3 modes at 1556 and 1546 cm^{-1} discussed in the previous paragraph. This is contrary to the experimental observation. The relative intensities predicted by the 6-31G calculations are in better agreement with the experimental intensities.

The 1254 cm^{-1} experimental band has weak infrared absorption and strong Raman intensity which, by analogy with the 1262 cm^{-1} band of methyloxirane,[16] can be attributed to the ring C–C stretching motion. The 6-31G mode at 1391 cm^{-1}, the 6-311G mode at 1392 cm^{-1}, and the 6-31G** mode at 1400 cm^{-1} have strong Raman intensity and weak infrared absorption in accordance with the experimental observations. The calculations suggest that the dominant potential energy contributions for this vibration are from the C*–C* stretching and the methine bending force constants.

The next four lower frequency 6-31G modes at 1319, 1307, 1261, and 1240 cm^{-1} are seen to arise from the hydrogen motions

(21) Cianciosi, S. J.; Spencer, K. M.; Freedman, T. B.; Nafie, L. A.; Baldwin, J. E. *J. Am. Chem. Soc.* **1989**, *111*, 1913–1915. Freedman, T. B.; Spencer, K. M.; McCarthy, C.; Cianciosi, S. J.; Baldwin, J. E.; Nafie, L. A.; Moore, J. A.; Schwab, J. M. *Proceedings of VIIth International Conference on Fourier Transform Spectroscopy*, in press.

of the methyl and methine groups. The corresponding experimental bands are at 1154 and 1110 cm^{-1} in the infrared spectrum and at 1163 and 1113 cm^{-1} in the Raman spectrum. The 6-31G mode at 1319 cm^{-1} and the equivalent 6-311G mode at 1316 cm^{-1} have relatively small infrared absorption intensities and this is probably the reason for the absence of a vibrational absorption band at 1163 cm^{-1} corresponding to the 1163 cm^{-1} Raman band. The 6-31G** calculations, however, predict strong absorption intensity for the corresponding band at 1325 cm^{-1}. This appears to be unrealistic since the experimental spectrum does not show a strong absorption band. Therefore we adhere to the 6-31G and 6-311G predictions and associate the 1319 cm^{-1} 6-31G normal mode with the 1163 cm^{-1} experimental Raman band and the 1307 cm^{-1} 6-31G normal mode with the 1154 cm^{-1} experimental infrared band. The remaining two 6-31G modes with frequencies of 1261 and 1240 cm^{-1} are associated with the experimental infrared band at 1110 cm^{-1} which corresponds to the Raman band at 1113 cm^{-1}.

On the basis of the symmetry arguments, one would expect to see two bands due to the C*–O stretching motions and two bands due to the exocyclic C–C* stretching motions which result from the symmetric and antisymmetric combinations of the individual C*–O and C–C* stretches. The antisymmetric C–C* stretching motion with 6-31G frequency of 1138 cm^{-1} and a hydrogen bending mode with 6-31G frequency of 1091 cm^{-1} have nearly equal and fairly large absorption intensities. However, the experimental infrared spectrum does not show two equal intensity bands at 1022 cm^{-1}. If we assign the 1022 cm^{-1} band exclusively to the antisymmetric C–C* stretching motion, then it should be depolarized in the Raman spectrum, but the experimental Raman band at 1022 cm^{-1} is weakly polarized. Moreover, in the VCD spectrum (Figure 4) the 1022 cm^{-1} absorption band is associated with two oppositely signed (poorly resolved) VCD bands. On the basis of these observations, the 1022 and 1015 cm^{-1} bands are associated respectively with the antisymmetric C–C* and hydrogen-bending vibrations. It cannot be conclusively determined as to which one of these two bands belongs to the C–C* stretching motion. However, on the basis of the analysis of associated VCD signs (vide infra) the assignment of the 1022 cm^{-1} band to the C–C* stretching vibration is favored.

The 6-31G calculations suggest that the symmetric C–C* stretching, the symmetric C*–O stretching, and the antisymmetric C*–O stretching modes with frequencies of 956, 866, and 787 cm^{-1} appear next to each other in the decreasing order of frequency. Since the experimental Raman band at 886 cm^{-1} is strongly polarized, which correlates with the small depolarization ratio predicted for the 956 cm^{-1} 6-31G mode, the 886 cm^{-1} band in the experimental spectra is associated with the symmetric C*–C stretching motion. The next two lower frequency experimental Raman bands at 811 and 719 cm^{-1} and the corresponding infrared bands at 812 and 722 cm^{-1} are then conclusively assigned to the symmetric and antisymmetric C*–O stretching motions. These assignments are in pleasing agreement with those for methyloxirane, where also the antisymmetric C*–O stretching mode is predicted to have lower frequency than that for the symmetric C*–O stretching mode.[16,22] There are, however, some problems with the 6-31G** predictions for the frequency ordering of the three modes just discussed. Based on the potential energy distributions (Table II), the 6-31G** modes at 1003 and 854 cm^{-1} correspond to the symmetric and antisymmetric C*–O stretching motions. But unlike in the 6-31G predictions, they are separated by a mode at 893 cm^{-1} with a small depolarization ratio like that of the experimental 886 cm^{-1} Raman band. Therefore the frequency order of the 6-31G** modes with frequencies 1003 and 893 cm^{-1} appears to be incorrect. Also the description of the 6-31G** mode at 893 cm^{-1} does not correspond to that of the 6-31G mode at 956 cm^{-1}. Similar problems were noted for methyloxirane when polarization functions were added to the 6-31G basis set.[16]

(22) Polavarapu, P. L.; Hess, B. A., Jr.; Schaad, L. J. *J. Chem. Phys.* **1985**, *82*, 1705–1710.

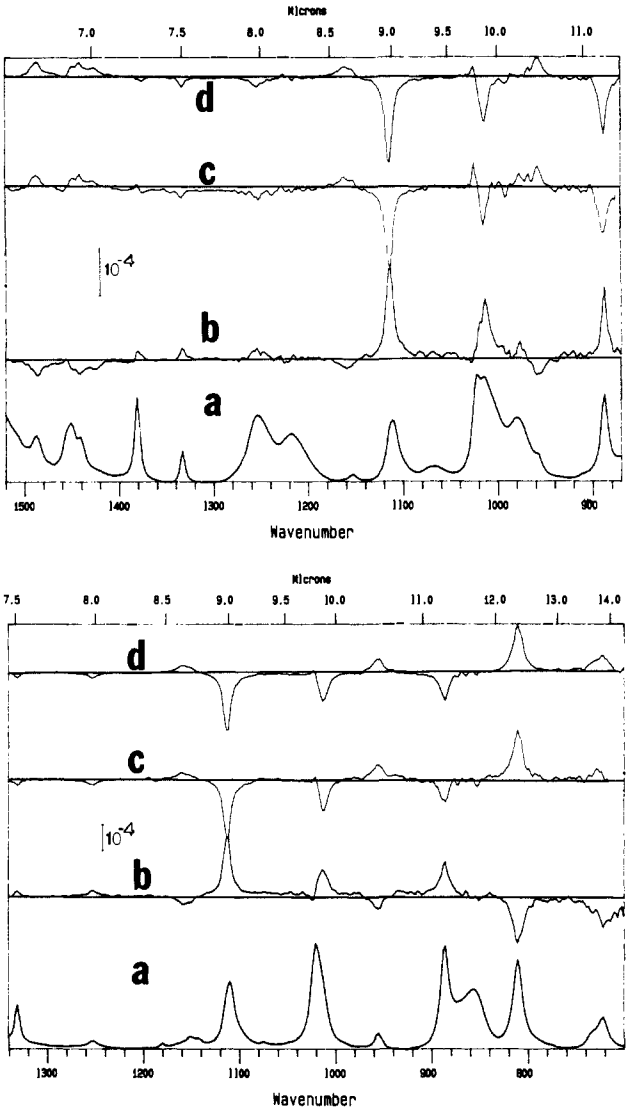

Figure 4. Experimental infrared absorption (a) and VCD (b, c, d) spectra of *trans*-2,3-dimethyloxirane at 4 cm^{-1} resolution. Spectrum b is for (−)-enantiomer and spectra c and d are for (+)-enantiomer; spectra b and c were obtained by subtracting the raw VCD of the racemic mixture from those of individual enantiomers; spectrum d was obtained by taking one-half of the difference between the raw VCD of (+)- and (−)-enantiomers. The absorption spectra were plotted on ~0 to 0.9 absorbance scale in A (top) and ~0 to 0.8 absorbance scale in B (bottom). The data acquisition time for the VCD spectrum of each sample is approximately 45 min. (A) 0.2 M CCl_4 solution; (B) 0.2 M CS_2 solution. VCD associated with the high-frequency shoulder of the 1452 cm^{-1} absorption band and that associated with the 1381 cm^{-1} absorption band are not definitive.

We should point out here that the 722 cm^{-1} band in the infrared spectrum has an overlapping intensity contribution from another weak band at about 735 cm^{-1}. It is not immediately obvious which one of these two should be attributed to the above-mentioned asymmetric C*–O stretching vibration. Since the 735 cm^{-1} band is relatively weak, we assume that this band originates in a nonfundamental vibration.

In the 500–100 cm^{-1} region, two exocyclic C–C*–O bending, two exocyclic C–C*–C* bending, and two methyl torsional modes are expected to be present. The 6-31G calculations predict one C–C*–O bending mode and one C–C*–C* bending mode, with frequencies of 499 and 498 cm^{-1}, to be nearly degenerate. The corresponding 6-311G and 6-31G** frequencies are 503 and 496 cm^{-1} and 516 and 490 cm^{-1}, respectively. All three calculations predict the lower frequency mode to have a very small absorption intensity and the higher frequency mode to have a small Raman intensity. These predictions are consistent with the experimental observation of an infrared absorption band at 473 cm^{-1} and of a Raman band at 466 cm^{-1} (with a hint of a higher frequency

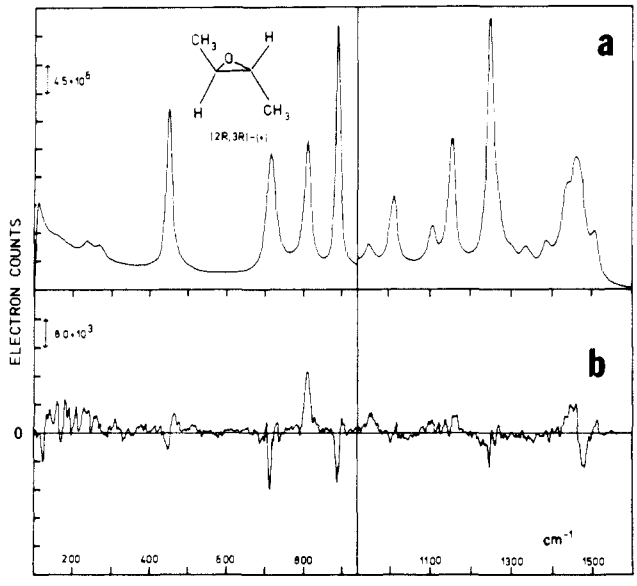

Figure 5. Experimental Raman ($I^R + I^L$, a) and ROA ($I^R - I^L$, b) spectra of *trans*-2,3-dimethyloxirane, measured in the backward scattering. The two regions, ~100–950 cm^{-1} and ~950–1600 cm^{-1}, are on slightly different scales.

shoulder). The next two 6-31G modes at 308 and 266 cm^{-1} are predicted to have weak Raman intensities, as are the corresponding 6-311G and 6-31G** modes at 306 and 268 cm^{-1} and at 302 and 267 cm^{-1}, respectively. These predictions concur with the weak Raman intensity for the experimental bands at 289 and 249 cm^{-1} (Figure 5). Although all calculations predict the major potential energy contribution for the first one of these bands, as expected, to arise from the C–C*–C* bending force constants, for the second band they predict the major potential energy contribution to arise from the torsional force constants rather than from the expected C–C*–O bending force constants. This may reflect incorrect relative magnitudes of force constants predicted by the ab initio calculations. The two lowest frequency Raman bands at ~200 and 185 cm^{-1} were assigned[12] to the torsional modes, which is supported by the mode descriptions of the lowest frequency ab initio vibrational motions.

The mode assignments suggested by Durig and co-workers[12] are included in Table V for comparison with the assignments derived from the potential energy distributions and atomic displacements obtained in the 6-31G calculation. There are several differences in these two different mode descriptions. Since there are significant differences between the theoretical and observed intensities for some bands, the assignments derived from the present ab initio calculations may require modifications in the future.

B. Vibrational Circular Dichroism. As the VCD associated with the vibrations arising from the H–C*–C*–H and C–C*–C*–C segments is of special interest we will consider them first. The C*–H stretching vibrations and the C–C*–C* bending vibrations fall outside of the experimental region investigated. Therefore the discussion is limited to the methine bending and C–C* stretching vibrations. On the basis of the ab initio calculations discussed in the previous section the experimental bands at 1489, 1335, and 886 cm^{-1} are assigned to symmetric methine bending, antisymmetric methine bending, and symmetric C–C* stretching vibrations, respectively. The vibrational frequencies of the antisymmetric C–C* stretching and a hydrogen-bending mode are predicted to be nearly equal. The corresponding experimental bands are identified to be at 1022 and 1015 cm^{-1}. Since these two bands are very close to each other, it is possible to associate the antisymmetric C–C* stretching vibration with either the 1022 cm^{-1} band or the 1015 cm^{-1} band, thus leaving an uncertainty.

The ab initio calculations suggest the dominant potential energy contributions for the symmetric methine bending mode to be associated with the H–C*–C* bending and C*–C* stretching force constants and those for the antisymmetric methine bending mode with the H–C*–C* and H–C*–O bending force constants. The ab initio calculations identify only these two as the primary methine bending vibrations. This is consistent with the identification of one methine bending vibration each in methyloxirane[22] and methylthiirane[23] and deviates from the assumption that two methine bending vibrations can be identified for each methine group. The dominant potential energy contributions for the antisymmetric C–C* stretching vibration are from the C–C* stretching force constants and those for the symmetric C–C* stretching vibration are from the C–C* as well as C*–O stretching force constants.

The theoretical VCD predictions derived[5] for the vibrations of an A_2B_2 molecule with C_2 symmetry can now be compared with the experimental observations. According to these predictions, the symmetric and antisymmetric vibrations are expected to have oppositely signed VCD with the sign pattern as follows: for a counterclockwise (CCW) A–B–B–A dihedral angle the symmetric vibration would have positive VCD and the antisymmetric vibration would have negative VCD. The experimental VCD observations (Figure 4) for the enantiomer with positive optical rotation are as follows: positive VCD for the symmetric methine bending vibration, negative VCD for the antisymmetric methine bending vibration, and negative VCD for the symmetric C–C* stretching vibration. These observations in conjunction with the above-mentioned theoretical predictions suggest a CCW dihedral angle for the H–C*–C*–H segment and a CW dihedral angle for the C–C*–C*–C segment. Since these angles in *trans*-2,3-dimethyloxirane correspond to the (2*R*,3*R*) configuration the VCD spectral data predict this configuration for the enantiomer with positive optical rotation. This is also the configuration derived several years ago by Schurig and co-workers[24] using complexation chromatography. In the above discussion we have not included the antisymmetric C–C* stretching vibration since this vibration can be associated with either the 1022 cm^{-1} or the 1015 cm^{-1} band. On the other hand if we apply the theoretical predictions to identify the antisymmetric C–C* stretching vibrational band, it is apparent that its assignment to the 1022 cm^{-1} band will be favored.

The conclusions reached above could in principle also be derived from the coupled oscillator (CO) theory.[3a] However, it can be shown convincingly that the CO mechanism is not prevalent for the vibrations considered. Similarly the fixed partial charge (FPC) mechanism[3b] can be ruled out because, if the FPC mechanism was dominant then the absorption intensities of the two methine bending vibrations should[5] have been in the ratio of 100:1 whereas their experimental intensities are nearly equal.

From the potential energy contributions mentioned earlier it is apparent that the additional internal coordinates participating in the symmetric methine bending vibration are different from those participating in the antisymmetric methine bending vibration. The same is true for the C–C* stretching vibrations. These differences are responsible for the observed frequency separation of the symmetric–antisymmetric pair of vibrations. Despite the presence of such differences in the internal coordinate compositions, which were not taken into account in the theoretical VCD predictions for A_2B_2 molecules, the observed VCD sign patterns are consistent with the predictions. This is precisely what is required if VCD spectroscopy is to serve as a reliable technique for determining absolute configurations.

The VCD associated with the ring C*–C* stretching vibration also appears to provide consistent configurational information. The corresponding band, observed at 1254 cm^{-1}, is negative for *trans*-(2*R*,3*R*)-dimethyloxirane (Figure 4), which is also the sign found for the associated band at 1262 of (*R*)-methyloxirane.[25] Similarly the band assigned to the antisymmetric ring C*–O stretching vibration is found to give positive VCD for *trans*-(2*R*,3*R*)-dimethyloxirane at 722 cm^{-1} as well as for (*R*)-

(23) Polavarapu, P. L.; Hess, B. A., Jr.; Schaad, L. J.; Henderson, D. O.; Fontana, L. P.; Smith, H. E.; Nafie, L. A.; Freedman, T. B.; Zuk, W. M. *J. Chem. Phys.* **1987**, *86*, 1140–1146.

(24) Schurig, V.; Koppenhoefer, B.; Buerkle, W. *J. Org. Chem.* **1980**, *45*, 538–541.

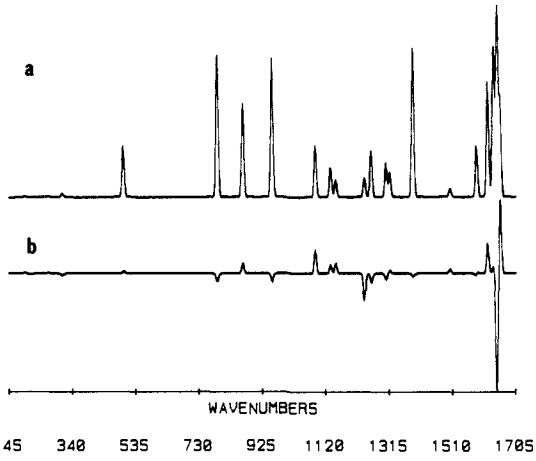

Figure 6. Ab initio Raman ($I^R + I^L$, a) and ROA ($I^R - I^L$, b) spectra of *trans*-(2*R*,3*R*)-dimethyloxirane obtained with the 6-31G basis set, for the backward scattering. The intensities are on an arbitrary scale.

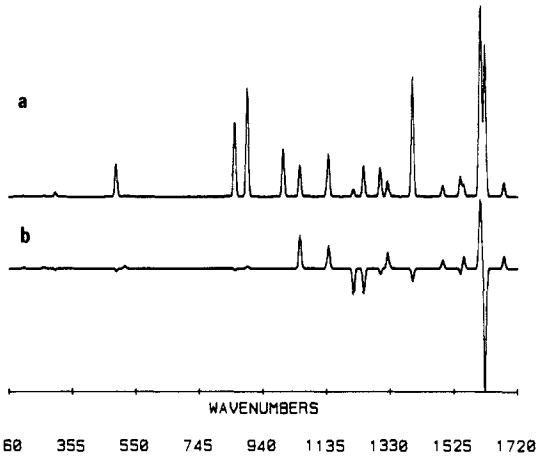

Figure 7. Ab initio Raman ($I^R + I^L$, a) and ROA ($I^R - I^L$, b) spectra of *trans*-(2*R*,3*R*)-dimethyloxirane obtained with the 6-31G** basis set, for the backward scattering.

methyloxirane[25] at 750 cm^{-1}. The VCD associated with the symmetric C*–O stretching vibration, however, is not consistent for these two molecules, because *trans*-(2*R*,3*R*)-dimethyloxirane has a large positive VCD for the corresponding band at 812 cm^{-1} while (*R*)-methyloxirane has only weak, uncertain VCD at 824 cm^{-1}.

Finally the hydrogen bending modes at 1154, 1110, 1015, and 959 cm^{-1} show fairly large VCD effects, but these are difficult to identify in the spectra of different molecules. VCD bands associated with the methyl deformation modes, at ~1452 cm^{-1}, again are unlikely candidates for a useful analysis because of the overlapping contributions from four different vibrations. Furthermore, since no significant VCD is associated with the methyl umbrella type mode, at 1381 cm^{-1}, it is unlikely that the methyl groups will serve as useful probes for VCD analysis.

In recent years ab initio VCD calculations[26,27] have become possible with use of closed expressions[28,29] as well as vibronic theoretical expressions.[30] Although the CADPAC program that we used for ROA calculations can provide the ab initio VCD intensities, we will not investigate them here as other groups[27,28,31,32] are actively involved in that aspect.

C. Raman Optical Activity. The ab initio ROA predictions for *trans*-(2*R*,3*R*)-dimethyloxirane obtained with the 6-31G and 6-31G** basis sets are summarized in Table VI. In order to assess the basis set influence on the normal coordinates and the Cartesian polarizability derivatives individually, we have also carried out calculations with mixed basis sets. That is, normal coordinates obtained with the 6-31G** basis set at the 6-31G** minimum energy geometry are combined with the Cartesian polarizability derivatives obtained with the 6-31G basis set at the 6-31G minimum energy geometry, keeping the same orientation of Cartesian axes in both calculations. This mixed calculation is labeled 6-31G**/6-31G. A similar but reverse calculation, namely the normal coordinates obtained with the 6-31G basis set and the Cartesian polarizability derivatives obtained with the 6-31G** basis set, is labeled 6-31G/6-31G**. The results of these two calculations are presented in Table VII.

Since the electric dipole–magnetic dipole polarizability tensor $G'_{\alpha\beta}$ is gauge dependent,[20] we have also investigated the influence of the gauge origin by using two different gauge origins. In one calculation the origin of the coordinate system and of the gauge are set at the center of charge of the nuclei, while in the second calculation they are set at the oxygen atom. These results are included in Table VI.

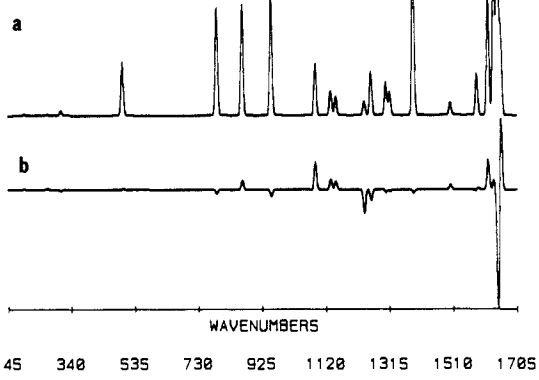

Figure 8. Ab initio Raman ($I^R + I^L$, a) and ROA ($I^R - I^L$, b) spectra of *trans*-(2*R*,3*R*)-dimethyloxirane, obtained with the 6-31G normal coordinates and 6-31G** Cartesian polarizability derivatives, for the backward scattering.

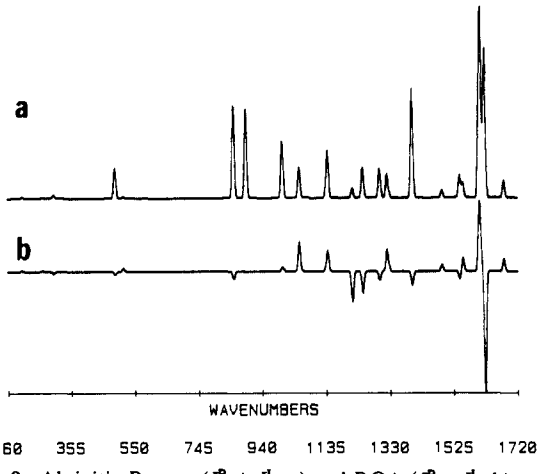

Figure 9. Ab initio Raman ($I^R + I^L$, a) and ROA ($I^R - I^L$, b) spectra of *trans*-(2*R*,3*R*)-dimethyloxirane, obtained with 6-31G** normal coordinates and 6-31G Cartesian polarizability derivatives, for the backward scattering.

The experimental Raman and ROA spectra obtained in the backward scattering geometry are shown in Figure 5. We have also recorded the depolarized and polarized ROA spectra in the 90° scattering geometry but these are not presented. The discussion in the following paragraphs will pertain to the unnor-

(25) Polavarapu, P. L. *Chem. Phys. Lett.* **1989**, *161*, 485–490.
(26) Amos, R. D.; Handy, N. C.; Jalkanen, K. J.; Stephens, P. J. *Chem. Phys. Lett.* **1987**, *133*, 21–26.
(27) Dutler, R.; Rauk, A. *J. Am. Chem. Soc.* **1989**, *111*, 6957–6966.
(28) Stephens, P. J. *J. Phys. Chem.* **1985**, *89*, 748–752.
(29) Buckingham, A. D.; Fowler, P. W.; Galwas, P. A. *Chem. Phys.* **1987**, *112*, 1–14.
(30) Nafie, L. A.; Freedman, T. B. *J. Chem. Phys.* **1983**, *78*, 27–31.
(31) Dothe, H.; Lowe, M. A.; Alper, J. S. *J. Phys. Chem.* **1988**, *92*, 6246–6249.
(32) Amos, R. D.; Handy, N. C.; Drake, A. F.; Palmieri, P. *J. Chem. Phys.* **1988**, *89*, 7287–7297.

Table VI. Theoretical and Experimental ROA Parameters[a] for *trans*-(2*R*,3*R*)-Dimethyloxirane

6-31G basis set							6-31G** basis set				experimental			
	$\Delta_\alpha \times 10^4$							$\Delta_\alpha \times 10^4$				$\Delta_\alpha \times 10^4$		
	origin at O atom			origin at center of charge				origin at center of charge						
freq, cm^{-1}	*Z*	*X*	180	*Z*	X	180	freq, cm^{-1}	*Z*	*X*	180	freq, cm^{-1}	*Z*	*X*	180
1661	16.4	22.8	43.5	16.0	22.4	42.8	1682	35.6	18.4	29.9	1487	+4.0	+	+5.7
1652	−14.0	−18.1	−33.8	−13.7	−17.8	−33.4	1623	−19.1	−24.3	−45.1				
1649	−1.4	−14.1	−33.1	−1.5	−14.2	−33.1	1620	11.1	9.8	15.9				
1640	−0.9	0.7	2.2	−0.8	0.8	2.4	1610	1.9	4.1	8.6	1445	−2.2	−	−5.3
1622	4.9	6.7	11.7	6.0	7.6	13.4	1606	6.4	8.0	14.5	1426	+5.9	+	+6.7
1588	14.3	15.2	26.7	14.6	15.6	27.4	1556	17.6	19.3	34.2	1381	−6.1	+	*b*
1587	−7.7	−8.8	−15.6	−6.2	−7.2	−13.0	1546	−4.8	−5.5	−9.9	1381	−6.1	+	*b*
1505	12.2	14.1	25.5	11.6	13.6	24.6	1493	10.6	13.4	25.0	1335	+5.0	+	*b*
1391	0.0	0.2	0.8	−1.6	−1.0	−1.0	1400	−3.1	−2.2	−3.5	1254	−4.3	*c*	−2.5
1319	26.9	2.3	9.0	22.2	1.1	7.0	1325	35.4	15.8	34.0	1163	+8.0	+	+2.7
1307	−4.0	−4.9	−9.1	−3.8	−4.8	−8.8	1302	−3.5	−3.8	−6.6				
1261	−4.9	−6.8	−12.9	−3.3	−5.2	−10.2	1250	−10.5	−13.6	−26.2	1113	+9.1	+	+10.3
1240	−29.5	−39.2	−73.9	−29.8	−39.5	−74.4	1218	−55.1	−69.7	−129.4	1113	+9.1	+	+10.3
1154	25.7	15.9	33.1	23.7	15.2	32.3	1141	12.1	11.1	23.9	1022	−3.7	−	*d*
1138	1.6	7.7	17.5	0.2	6.4	15.2	1141	−0.7	4.4	10.9	1022	−3.7	−	*d*
1091	6.5	12.2	24.8	6.2	11.9	24.4	1055	10.4	17.4	34.8	960	+7.9	+	+2.7
956	−6.6	−3.1	−3.2	−6.5	−2.9	−3.2	893	−0.1	−0.1	0.6	886	−5.0	*c*	−5.7
866	2.9	3.4	6.2	2.6	3.1	5.6	1003	1.8	−0.8	0.0	811	+3.7	+	+9.9
787	−0.2	−1.3	−3.1	−0.1	−1.2	−2.9	854	1.8	0.2	−0.9	719	+2.3	−	−6.2
499	12.5	17.2	32.7	14.0	18.9	35.7	516	34.7	48.5	92.6	473	+6.2	+	+7.4
498	−0.4	0.9	−1.9	−0.1	1.0	−1.7	490	−1.6	0.3	−2.8	466	−4.2	−	−1.9
308	−3.4	−9.1	−19.4	−3.2	−9.0	−19.3	302	−2.7	−6.8	−14.4	289	+8.8	+	+[b]
266	13.2	15.4	28.1	13.1	15.7	29.4	267	15.0	16.7	33.7	249	+13.1	+	+[b]
211	−29.6	−29.2	−49.7	−33.6	−30.6	−50.4	224	−20.0	−16.1	−25.1	200	*d*	*d*	*d*
193	32.8	25.0	37.2	30.5	22.2	31.6	203	31.2	20.4	26.1	185	+10[e]	*d*	*d*

[a] Δ_α, for $\alpha = Z, X$ and 180 are defined in eqs 1–3. The former two correspond to the normalized depolarized and polarized ROA in the 90° scattering, while the latter corresponds to the normalized ROA in the backward scattering. For Δ_x, experimental magnitudes are not listed due to the presence of off-sets, which introduce large uncertainties. [b] Weak feature. [c] Polarization artifact. [d] Uncertain. [e] From ref 10.

Table VII. Evaluation[a] of the Basis Set Influence on Cartesian Polarizability Derivatives and Normal Modes

6-31G/6-31G**						6-31G**/6-31G					
	Raman Intensities		$\Delta_\alpha \times 10^4$				Raman intensities		$\Delta_\alpha \times 10^4$		
freq, cm^{-1}	$45\alpha^2 + 4\beta(\alpha)^2$	$3\beta(\alpha)^2$	*Z*	*X*	180	freq, cm^{-1}	$45\alpha^2 + 4\beta(\alpha)^2$	$3\beta(\alpha)^2$	*Z*	*X*	180
1661	5.5	3.9	20.0	26.6	50.2	1682	2.9	0.4	25.2	13.4	21.8
1652	10.1	7.6	−16.0	−20.0	−37.0	1623	11.5	8.6	−16.4	−21.7	−40.9
1649	2.6	2.0	−3.8	−15.9	−35.7	1620	6.5	4.8	10.8	9.3	14.8
1640	9.7	7.2	−0.0	1.6	3.7	1610	13.0	9.7	0.9	3.2	6.9
1622	8.3	5.4	6.3	7.8	13.7	1606	12.5	8.8	5.7	7.5	13.9
1588	0.8	0.6	17.3	18.8	33.2	1556	1.6	1.2	14.1	14.8	25.8
1587	1.9	1.4	−5.8	−6.8	−12.5	1546	2.5	1.8	−5.1	−5.8	−10.5
1505	0.8	0.6	8.5	10.4	19.2	1493	0.8	0.6	11.0	14.1	26.2
1391	12.9	5.0	−1.6	−0.7	−1.0	1400	14.6	5.5	−3.1	−2.6	−3.6
1319	2.0	0.3	4.8	−3.7	−4.9	1325	3.7	0.6	30.9	11.1	27.2
1307	2.0	1.5	−2.1	−2.7	−5.1	1302	3.0	2.3	−4.8	−5.1	−9.0
1261	2.6	1.8	−4.8	−7.2	−14.2	1250	3.2	2.3	−6.7	−10.7	−21.1
1240	0.8	0.6	−41.2	−52.7	−98.3	1218	1.0	0.7	−37.6	−49.2	−92.3
1154	1.4	0.4	16.6	11.2	25.2	1141	2.4	0.9	14.5	11.9	24.6
1138	1.4	1.1	5.3	11.1	23.1	1141	2.9	2.1	−3.6	1.2	5.4
1091	2.9	2.2	9.2	15.5	30.9	1055	3.0	2.3	7.2	13.5	27.6
956	10.5	1.5	−5.9	−3.2	−3.1	893	10.3	4.6	−0.9	−0.7	−0.3
866	6.3	4.3	2.7	2.8	4.7	1003	7.8	1.9	3.0	0.8	2.3
787	5.9	4.4	0.6	−0.7	−2.0	854	9.0	6.8	1.0	−0.7	−2.3
499	0.2	0.1	13.8	19.4	37.2	516	0.1	0.1	27.2	37.2	70.7
498	3.6	0.8	−0.4	0.7	−1.8	490	3.8	0.9	−1.2	0.5	−2.9
308	0.2	0.2	−3.6	−8.4	−17.6	302	0.3	0.2	−2.5	−7.5	−16.2
266	0.1	0.1	15.2	15.3	30.4	267	0.1	0.1	13.1	17.7	34.0
211	0.0	0.0	−15.1	−14.1	−23.5	224	0.0	0.0	−37.1	−30.5	−48.0
193	0.1	0.0	37.0	24.4	32.3	203	0.1	0.1	25.5	17.7	25.0

[a] These calculations were done with the origin at the center of charge. The 6-31G**/6-31G calculations were also done with the origin at the oxygen atom. But the resulting values do not significantly differ from the values given here.

malized ROA in the backward scattering shown in Figures 5–9. The normalized ROA values, Δ, can be found in Table VI.

The 6-31G methine bending mode at 1661 cm^{-1} is predicted to show a positive ROA for the (2*R*,3*R*)-enantiomer, which is also the sign observed for the corresponding experimental band at 1487 cm^{-1}. The next three 6-31G ROA modes at 1652, 1649, and 1640 cm^{-1} are negative, negative, and positive, respectively, and the combined effect of these three modes corresponds to the negative ROA at 1445 cm^{-1} in the experimental spectrum. The 6-31G ROA for the 1622 cm^{-1} mode and the corresponding experimental ROA at 1426 cm^{-1} are also in agreement, both being positive. The two near-degenerate methyl bending modes with the 6-31G frequencies of 1588 and 1587 cm^{-1} have opposite ROA signs leading to mutual cancellation. The corresponding experimental ROA band at 1381 cm^{-1} is also very weak. The methine antisymmetric bending mode with 6-31G frequency of 1505 cm^{-1} is predicted to have small positive ROA, while in the experimental spectrum the corresponding ROA band at 1335 cm^{-1} is not clearly defined.

For the experimental bands discussed in the previous paragraph, the 6-31G** predictions of net ROA sign patterns are identical with the 6-31G predictions with one exception. The two 6-31G** methyl bending modes at 1556 and 1546 cm^{-1} are well separated and exhibit a bisignate ROA couplet (Figure 7), and these predictions are not in agreement with the experimental observations.

The 6-31G ROA predictions for the ring C*–C* stretching vibration at 1391 cm^{-1} are influenced by the choice of origin. With the gauge origin set at the oxygen atom, a small positive ROA was predicted for this band. However, when the gauge origin was set at the center of charge of the nuclei the associated ROA was predicted to be negative. In the experimental ROA spectrum, the corresponding band at 1254 cm^{-1} is negative and weak. The 6-31G** calculations also predict negative ROA for this band.

For the next three pairs of 6-31G modes, namely those at 1319 and 1307 cm^{-1}, 1261 and 1240 cm^{-1}, and 1154 and 1138 cm^{-1}, the net ROA sign pattern does not match the one seen in the experimental spectrum. These three pairs of ROA bands give rise to a net negative, negative, positive sign pattern while in the experimental ROA spectrum the corresponding bands at 1163, 1113, and 1022 cm^{-1} have weak positive, positive, and uncertain (possibly negative) signs, respectively. In the 6-31G** calculation, the first pair of modes at 1325 and 1302 cm^{-1} have a net positive ROA which matches with the experimental sign for the corresponding band at 1163 cm^{-1}. The ROA associated with the remaining two pairs of 6-31G** modes at 1250 and 1218 cm^{-1} and 1141 and 1141 cm^{-1} does not agree with the experimental observations.

The positive ROA sign observed for a hydrogen-bending band at 960 cm^{-1} is predicted correctly by the 6-31G as well as by the 6-31G** calculations, where the corresponding bands are at 1091 and 1055 cm^{-1}, respectively. The symmetric C–C* stretching band in the experimental spectrum, at 886 cm^{-1}, has negative ROA. The 6-31G calculations predict negative ROA for the corresponding mode at 956 cm^{-1}, supporting the experimental observation.

The next two 6-31G modes at 866 and 787 cm^{-1}, respectively due to the symmetric and antisymmetric C*–O stretching vibrations, are predicted to have positive and negative ROA signs, respectively. These predictions are in excellent agreement with the experimental observations where the corresponding bands are 811 and 719 cm^{-1}. In the 6-31G** calculations, we mentioned earlier that there are some uncertainties in the mode descriptions of the symmetric C*–C and C*–O vibrations. Although the 6-31G** calculations also predict a correct ROA sign pattern for the two C*–O stretching bands, the relative ROA magnitudes (Figure 7) are quite weak.

One important experimental observation is that the ROA associated with the antisymmetric C*–O stretching band changes sign from the polarized to the depolarized measurement.[11] Both of the mixed calculations, 6-31G/6-31G** and 6-31G**/6-31G, correctly predict the sign reversal (Table VII) matching the experimental observation. This trend is only apparent for the 6-31G band at 787 cm^{-1} as the associated unnormalized depolarized ROA magnitude is much smaller than that of the polarized ROA. However, the 6-31G** calculation is in hopeless disagreement with the experiment because it predicts the sign reversal for the *symmetric* C*–O stretching mode, which is not observed.[11]

A positive–negative couplet is present in the experimental ROA spectrum at ~466 cm^{-1}. The 6-31G calculations predict the same sign pattern for the bands at 499 and 498 cm^{-1}, but since the band positions are not well-separated, the bisignate pattern is not apparent in the simulated spectrum. In the 6-31G** calculation, these bands are better separated, now being at 516 and 490 cm^{-1}, and the positive–negative couplet is clearly visible in the simulated spectrum.

For the remaining four experimental Raman bands at 289, 249, 200, and 185 cm^{-1}, the associated ROA in backward scattering (Figure 5) is not clearly established due to the interference from the stray light. However, in the depolarized ROA measurements the ROA signs for three of these bands were determined. In particular, for the symmetric methyl torsional mode negative depolarized ROA was observed[10] for the (2*S*,3*S*)-enantiomer. This is in agreement with the positive depolarized ROA predicted for the same vibration of (2*R*,3*R*)-enantiomer by both the 6-31G as well as 6-31G** calculations with frequencies of 193 and 203 cm^{-1}, respectively.

Now we would like to address the influence of the choice of gauge origin for ROA calculations. In eqs 1–3, the normal coordinate derivatives of electric dipole–magnetic dipole polarizability tensors are required, and these tensors are dependent[20] on the choice of gauge. From the two sets of values presented in Table VI with the 6-31G basis set, one with the origin at the oxygen atom and the other with the origin at the center of charge of the nuclei, it is clear that the differences among these two calculations are very minor. The only vibration for which we noted any significant difference is that at 1391 cm^{-1}. For this case the ROA sign obtained in the calculation with the origin at the center of the charge of nuclei is in agreement with the experimental observation. Similarly the mixed 6-31G**/6-31G calculations (Table VII) did not show any significant influence on the choice of gauge origin.

Table VII summarizes the mixed basis set calculations. In the mixed calculation labelled 6-31G/6-31G** the normal modes are obtained with the 6-31G basis set and the Cartesian polarizability derivatives are obtained with the 6-31G** basis set. If these results are significantly different from those obtained entirely with the 6-31G basis set (Table VI) then it would imply that the Cartesian polarizability derivatives obtained with the 6-31G and 6-31G** basis sets differ from each other significantly. Similar analysis can be obtained by comparing the results obtained in the 6-31G**/6-31G mixed calculation with those obtained entirely with the 6-31G** basis set. In order to provide a visual comparison, the backward scattered Raman and ROA spectra obtained in the 6-31G/6-31G** and 6-31G**/6-31G calculations are shown in Figures 8 and 9, which can be compared with those in Figures 6 and 7, respectively. From this comparison it is apparent that the 6-31G/6-31G** results are very similar to the 6-31G results. Also, the 6-31G**/6-31G results are similar to the 6-31G** results. We previously reached a similar conclusion for methyloxirane[16] which indicates that the Cartesian polarizability derivatives are not significantly influenced by the polarization functions added to the 6-31G basis set. However, these polarization functions influence the structural parameters and hence the force constants (see Tables I and III) thereby leading to significant variations in the normal mode compositions.

In particular, we find that the ab initio Raman and ROA predictions obtained with the 6-31G basis set are in reasonable agreement with the experimental observations. The addition of polarization functions to the 6-31G basis set leads to shorter C–O bond lengths and significantly deteriorated normal vibrations involving these bonds. These conclusions are consistent with the results obtained for methyloxirane.[16]

Finally, a few comments on the comparative assessment of VCD and ROA are in order. One should view ROA and VCD as complementary techniques since for bands where VCD is not particularly informative, ROA appears to provide unique information and vice versa. The polarized ROA patterns associated with the symmetric and antisymmetric C*–O stretching vibrations of *trans*-2,3-dimethyloxirane are configurationally consistent[11] with those of methyloxirane; for the *R*-enantiomers the symmetric vibration has positive ROA and the antisymmetric vibration has negative. The same configurationally consistent ROA was also observed for the C*–S stretching vibrations of methylthiirane.[11,15] Furthermore, the polarized and depolarized ROA associated with the antisymmetric C*–O stretching vibration of *trans*-2,3-dimethyloxirane are of opposite signs.[11] This unusual sign reversal, for a given ROA band, from the polarized to the depolarized measurement can be interpreted as resulting from the dominant electric quadrupole polarizability contribution from the Rydberg electronic levels: an extensive discussion of this aspect is given elsewhere.[11]

Unlike in VCD, the methine bending and C–C* stretching vibrations do not seem to be of much significance for a configu-

rational analysis based on ROA measurements. In the experimental backscattered ROA spectrum, the 1487 cm^{-1} band due to the symmetric methine bending motion is positive for the (2*R*,3*R*)-enantiomer while that at 1335 cm^{-1} due to the antisymmetric methine bending mode is of uncertain sign. Similarly the backscattered ROA associated with the symmetric C–C* stretching vibration at 886 cm^{-1} is negative, but that associated with the antisymmetric C–C* stretching, at 1022 cm^{-1}, is uncertain. Therefore, it is not possible to carry out a configurational analysis for this molecule using the simple two-group model for ROA. The ring C*–C* stretching vibrational band at 1254 cm^{-1}, which was noted in the previous section to yield configurationally consistent VCD for *trans*-2,3-dimethyloxirane and methyloxirane, is also not particularly useful for ROA analysis. This is because ROA associated with this band is negative for *trans*-(2*R*,3*R*)-dimethyloxirane but is uncertain for (*R*)-methyloxirane. However, this conclusion is subject to the control of polarization artifacts in ROA measurements. More favorable conclusions on the ROA associated with the ring C*–C* and symmetric C–C* vibrations might emerge, if improvements in the backscattering ROA measurements can reduce artifacts for the strongly polarized Raman bands even further.

For the low-frequency vibrations, such as methyl torsional vibrations, VCD measurements are not yet feasible. Although preliminary CD measurements in the millimeter[33] wavelength region have been carried out more progress is required for VCD measurements on methyl torsion vibrations. On the contrary, ROA measurements for these vibrations are routine.[10] In addition, the inertial methyl torsion model[10] appears to be very useful since it gives the correct sign and approximate magnitude for the experimental symmetric methyl torsion ROA band at 185 cm^{-1}. This further emphasizes the complementarity between VCD and ROA since methyl torsions are likely to remain inaccessible to VCD measurements for some time.

IV. Summary

We have presented the experimental VCD and ROA spectra for *trans*-2,3-dimethyloxirane. Ab initio vibrational frequencies, infrared absorption, and Raman intensities obtained with 6-31G, 6-311G, and 6-31G** basis sets were used to identify the experimental bands due to different vibrational modes. Although there are some serious disagreements between the calculated and observed vibrational intensities (infrared as well as Raman), the ab initio vibrational predictions provided guidelines to infer the vibrational assignments for the experimental bands. The vibrational assignments obtained with the 6-31G basis set appeared to correlate with the experimental data better than those obtained with the 6-31G** basis set. The C–O bond lengths obtained with the 6-31G** basis set are considerably shorter and may have led to unreliable relative magnitudes for force constants, which in turn led to doubtful frequency ordering and normal mode composition for some vibrational bands.

The experimental VCD data associated with the symmetric methine bending, antisymmetric methine bending, and symmetric C–C* stretching bands are interpreted with the help of theoretical VCD expressions derived for A_2B_2 molecules of C_2 symmetry. This analysis indicated that the enantiomer with positive optical rotation should have (2*R*,3*R*) configuration, which is also the observation made by Schurig and co-workers using complexation chromatography. This agreement further establishes the role of VCD in deducing molecular stereochemistry.

The experimental ROA and VCD spectra were found to be of complementary nature, in providing the structural information. Those vibrational bands, which did not have measurable or easily interpretable VCD, were found to have significant and useful ROA features. Similarly those vibrational bands whose ROA is uncertain due to polarization artifacts or small magnitudes, were found to have useful VCD features.

The ab initio ROA spectrum obtained with the 6-31G basis set was found to have the correct signs for most of the vibrational bands. The 6-31G** ROA spectrum did not show any significant improvement over the 6-31G ROA spectrum. Instead, the uncertainties in the frequency ordering of 6-31G** modes introduced additional difficulties in analyzing the experimental data. The predicted ROA magnitudes, normalized with the Raman intensity, appeared in general to be larger than the experimental values. The ab initio ROA predictions were not influenced significantly by two different choices made for the gauge origin in evaluating the $G'_{\alpha\beta}$ tensors.

The mixed basis set calculations indicated that the normal modes of vibration are very sensitive to the variations among the 6-31G and 6-31G** basis sets. However, Cartesian polarizability derivatives were not found to be sensitive to these variations. These conclusions were deduced from the observation that the Raman as well as the ROA spectra obtained with the 6-31G and 6-31G/6-31G** calculations remained nearly identical. A similar observation was found to be true for the 6-31G** and 6-31G**/6-31G calculations. Thus it appears that, at the SCF level, it is necessary to establish the normal modes more accurately than the Cartesian polarizability derivatives.

Acknowledgment. Grants from NIH (GM29375), NSF (CHE8808018), SERC, Wolfson Foundation, and Deutsche Forschungsgemeinschaft (III02-He 1588/1-1) are gratefully acknowledged.

Note Added in Proof. In presenting the theoretical Raman and ROA spectra it is necessary to include, along with $(\nu_0 - \nu_i)^4$, the vibrational frequency (ν_i) dependent terms $h/8\pi^2 c\nu_i$ and $1/1 - \exp(-hc\nu_i/kT)$. These two terms were inadvertantly omitted. Although none of our conclusions will be affected by this omission, the actual theoretical spectra will be slightly different in that the bands around 1600 cm^{-1} will be slightly less intense and those around 400 cm^{-1} will be slightly more intense, on a relative scale, than they appear in Figures 3 and 6–9.

Registry No. (–)-*trans*-(2*S*,3*S*)-Dimethyloxirane, 63864-69-7; (+)-*trans*-(2*R*,3*R*)-dimethyloxirane, 1758-32-3.

(33) Polavarapu, P. L.; Quincey, P.; Birch, J. R. *Infrared Phys.*, in press.